IEEE Access
Multidisciplinary | Rapid Review | Open Access Journal

Received 2 June 2022, accepted 17 June 2022, date of publication 23 June 2022, date of current version 29 June 2022.

Digital Object Identifier 10.1109/ACCESS.2022.3185730

Automatic Detection and Tracking of Random Frequency Signals Using Magnitude and Phase Information

DRAGANA CAREVIC
Maritime Division, Defence Science and Technology Group, HMAS Stirling, Rockingham, WA 6168, Australia
e-mail: dragana.carevic@defence.gov.au

ABSTRACT This paper presents an approach to the problems of detection and frequency estimation of a frequency modulated narrow-band signal in additive complex Gaussian noise. The signal is assumed to have an unknown amplitude, initial phase and frequency trajectory over time, while *a priori* information regarding random frequency variability is taken to be available. The proposed approach operates in the frequency domain and uses the magnitude and phase of the discrete-time Fourier transforms computed over nonoverlapping signal segments. Robustness at low signal-to-noise ratios is achieved by suppressing the segment-related likelihoods for which the phase estimation error is large. The approach utilises unthresholded transform data and thus works in a track-before-detect manner, and the frequency trajectory is estimated by applying a search over the frequency-time bins. The results of a simulation study involving two signal types with different frequency variability are described.

INDEX TERMS Detection algorithms, frequency estimation, Markov processes, maximum a posteriori estimation, phase frequency detectors, phase estimation, signal detection, signal processing algorithms, state estimation, Viterbi algorithm.

I. INTRODUCTION

Detection and accurate estimation and tracking of time-varying frequency signals embedded in background noise is a problem that is important in diverse fields such as seismology, radar, sonar, telecommunications and astronomy. The signals are characterised by a slowly varying amplitude and a phase that is represented by an integral of frequency over time. In this way, both amplitude and phase contain important information that can be used for signal estimation. However, phase is particularly susceptible to noise, and at very low signal-to-noise ratios (SNRs), highly robust methods are needed for its estimation.

A number of frequency tracking algorithms have been proposed in the literature. A popular approach is to apply the discrete Fourier transform (DFT) to nonoverlapping segments of the received discrete time series, obtaining, as a result, the DFT magnitudes and phases related to the signal segments. A hidden Markov model (HMM) is usually applied to represent the probabilistic transition of discrete frequency states in consecutive data blocks [1]–[9]. Other techniques rely on maximum *a posteriori* (MAP) estimation, where the prior probability of discrete frequency state transition is modelled using a Markov chain [10]. An alternative approach is to model the frequency state space as being continuous and to apply sequential frequency estimation in either the frequency or time domain. Examples include the methods using the histogram probabilistic multihypothesis tracking (H-PMHT) algorithm [11], [12], Dirichlet process mixture model [12], extended Kalman filtering [13] and particle filter [14], [15]. Notably, most of these techniques use only the magnitude and discard the valuable information that is contained in the signal phase.

There are also many techniques that can accurately estimate instantaneous frequency and that use the signal phase information. Peleg and Friedlander [16], [17] described the discrete polynomial-phase transform (DPT) for polynomial phase (PF) models and used it to estimate PF signal parameters. In addition, the discrete fractional Fourier transform (DFrFT) [18], [19] has been proposed as a tool for processing linear frequency modulated (LFM) signals. The high computational complexity of the DFrFT has been subsequently reduced by the introduction of the sparse DFrFT (SDFrFT) [20], [21]. This algorithm simultaneously

The associate editor coordinating the review of this manuscript and approving it for publication was Gerard-Andre Capolino.

computes the transform of and detects the signals that are sparsely represented in the fractional Fourier domain. The detection and estimation of more general phase signals is achieved by using the short-time fractional Fourier transform (STFrFT) [22]. This transform is equivalent to applying the conventional short-time Fourier transform (STFT) on the signals using a FrFT window. The references [23]–[25] describe short-time polynomial phase modelling of the signals representing vocalizations of marine mammals. The authors were able to accurately track nonlinear time-frequency signal components and extract the time-phase information. Similarly, Liu *et al.* [26] applied DPT to nonoverlapping signal segments to estimate multiple signal chirp rates and used SDFrFT with different rotation angles to determine the initial frequencies of a multicomponent signal. While these techniques can estimate the instantaneous frequency with high accuracy, their drawback is that they are not robust enough to be applicable to signals at a low SNR.

Recently, Suvorova *et al.* [9] derived a joint probability density function (pdf) that models the frequency and phase evolution of a random frequency signal and used this density to compute the transition probabilities of a phase-frequency Markov chain. The authors also described an application of an HMM phase-frequency approach to the detection of a randomly wandering tone at low SNR. However, the information presented in [9] is not detailed enough for their approach to be replicated.

This paper presents a robust method for the detection and tracking of slowly varying instantaneous frequencies at low SNRs using phase and magnitude information. A posterior pdf that is a function of both the magnitude and phase of the discrete-time Fourier transforms (DTFT) computed over nonoverlapping signal segments is derived. The discrete phase-frequency states are defined to coincide with the DTFT frequency-time bins, and the transition of the discrete states is modelled using a first-order homogeneous Markov sequence. The likelihood used by the posterior pdf depends on pairs of the DTFT phases computed for consecutive signal segments, and the robustness of the algorithm is achieved by suppressing the segment-related likelihoods with a considerable error in the DTFT phase estimation.

Known similarities to [9] are in the way the transition probabilities of the phase-frequency Markov chain are computed and in the use of a prior probability of signal amplitude. An important difference is that our approach utilises the posterior pdf described above, while [9] relies on an HMM.

Some applications of the proposed method include detection and estimation of narrow-band underwater acoustic signals radiated by ships and underwater vehicles due to harmonics of the engine speed and shaft/propeller rotation [27], estimation and tracking of the instantaneous spectrum of frequency hopping signals used in radar and telecommunication applications [28], and detection and tracking of gravitational waves with the application in astronomy [7].

The contribution of this paper includes two aspects. The first is the derivation of a robust posterior pdf that uses the DTFT magnitudes and phases of nonoverlapping signal segments. The DTFT phase is an estimate of the true signal phase and is highly sensitive to noise. The proposed posterior pdf suppresses the segment-related likelihoods for which the phase estimation error is large. This ensures that the algorithm can detect and track the instantaneous signal frequency and estimate phase information at a very low SNR.

The second contribution is the derivation of two algorithms suitable for the maximisation of this density. The Viterbi algorithm [2], [29] is applied to obtain the MAP estimate of the most likely sequence of the phase-frequency states. Additionally, a phase-frequency version of the forward-backward algorithm [1], [2] is presented. This is a smoothing algorithm that maximises the probability of the state at each time step given the observation sequence at all time steps. At the output, both algorithms also produce a statistic that is used for signal detection.

A comprehensive simulation study involving two signal types with different frequency variabilities was carried out using Monte Carlo simulations with additive white Gaussian noise. The results show that the proposed algorithms significantly improve the detection performance and frequency estimation accuracy compared to several existing frequency detection and tracking methods.

This paper is organised as follows. Section II presents the derivation of the posterior distribution for phase-frequency tracking that uses the DTFT of nonoverlapping signal segments. Section III describes the implementation of the DTFT-based estimation approach using the Viterbi and forward-backward algorithms. The results of testing the proposed methods using synthetic signals are shown in Section IV, and some concluding remarks are presented in Section V.

II. DERIVATION OF THE POSTERIOR DISTRIBUTION FOR PHASE-FREQUENCY ESTIMATION

This section defines a narrow-band continuous-time signal model that is used for phase-frequency tracking. Next, the derivation of a continuous-time posterior distribution of the signal model parameters is presented, followed by the derivation of this distribution in discrete time.

A. MODEL

An unknown complex signal with time-varying amplitude and phase is given by

$$s(t) = A(t)e^{j\phi(t)}, \qquad t_1 \le t \le t_f \tag{1}$$

where

$$\phi(t) = 2\pi \int_{t_1}^{t} f(\tau)d\tau \tag{2}$$

is the signal phase, and $f(t)$ is a time-varying frequency. Then, denote by $x(t)$ the signal corrupted by noise

$$x(t) = s(t) + n(t) \tag{3}$$

where $n(t)$ is complex white Gaussian noise with one-sided spectral level $\mathcal{N}_0$.

The signal phase is modelled as piecewise linear over consecutive nonoverlapping segments of length T, i.e., as

$$\tilde{\phi}(t) = \phi_k + 2\pi f_k(t - t_k), \qquad t_k \le t < t_{k+1} \tag{4}$$

$k = 1, \ldots, K$, where $\phi_k = \tilde{\phi}(t_k)$ is the phase at time t_k, f_k is the discrete frequency, $t_{k+1} - t_k = T$, and we assume that $t_1 = 0$. Similarly, the signal amplitude is approximated by a constant over each time interval

$$\tilde{A}(t) = A_k, \qquad t_k \le t < t_{k+1}. \tag{5}$$

The amplitude A_k, frequency f_k, and phase ϕ_k in (4)-(5) are the unknown parameters of the signal model that need to be estimated. The amplitude is taken to be a continuous random variable while the frequency f_k is a discrete random variable that takes values from a set $\mathcal{F} = \{\zeta_j\}_{j=1}^{J}$ where $\zeta_j = \zeta_1 + (j-1)\Delta f, j = 1, \ldots, J$. ζ_1 and ζ_J are the lowest and the highest frequencies of interest, respectively, and the adjacent frequencies in the set are related as $\zeta_j = \zeta_{j-1} + \Delta f$. The phase at t_k is given by $\phi_k = \phi_{k-1} + 2\pi f_{k-1} T$, where $f_{k-1} = \zeta_j \in \mathcal{F}$, and $2\pi f_{k-1} T$ is the phase increment over the $(k-1)$st time interval T. Therefore, ϕ_k is also discrete, with J possible discrete values for $f_{k-1} = \zeta_j, j = 1, \ldots, J$.

Although equation (4) models the signal frequency as a piecewise constant function of time, in reality, the frequency can vary over the segment length T. It is assumed that for the class of signals of interest, the frequency evolves continuously over time (for example, $f(t)$ obeys a stochastic process driven by white noise). This implies that the frequency change over a finite duration of time is bounded. To optimise the performance of the phase-frequency tracking, the frequency increment $\Delta f = \zeta_j - \zeta_{j-1}$ and the time interval T used in the phase model (4) need to be selected such that the absolute value of the change of the signal frequency over the duration of T is less than or equal to Δf [9]. [10] shows that if the first derivative of the signal frequency is bounded, i.e., if $|\frac{df}{dt}| \le \beta/2\pi$, then the maximum length time interval $T = T_s$ can be found as $T_s = \sqrt{2\pi/\beta}$, and the corresponding (maximum) change of the signal frequency over T_s is $\Delta f_s = 1/T_s$. Accordingly, $T_s \Delta f_s = 1$ and T_s can be seen to be the characteristic time interval that depends on the frequency variability [10].

If Δf is chosen such that $T\Delta f = 1$ and $T \le T_s$, then, due to the variability of the frequency, the difference between the actual signal phase and the model (4) (or the loss of phase coherence) over T is within $\pm\pi\Delta f T = \pm\pi$. This is too large for reliable phase-frequency tracking, and smaller values for Δf and ΔT are needed. Therefore, we set $\Delta f < \Delta f_s$ and select T such that $T \le \frac{\Delta f}{\Delta f_s} T_s$. In this case, $T\Delta f < 1$, and the change in the signal frequency over T remains within $\pm\Delta f$.

B. CONTINUOUS-TIME POSTERIOR DISTRIBUTION FOR PHASE-FREQUENCY ESTIMATION

The estimated sequence of the signal parameters $\{\hat{A}_k, \hat{\phi}_k, \hat{f}_k\}_{k=1}^{K}$ can be obtained by maximising the following log-posterior distribution over A_k, ϕ_k, f_k [10], [30]

$$\begin{aligned}\log\left[\Lambda\left(\{A_k, \phi_k, f_k\}_{k=1}^{K}\right)\right] &\propto \frac{2}{\mathcal{N}_0}\mathrm{Re}\int_0^{KT} x(t)\overline{\tilde{s}(t)}dt - \frac{1}{\mathcal{N}_0}\int_0^{KT}|\tilde{s}(t)|^2 dt \\ &+ \log\left[p\left(\{A_k, \phi_k, f_k\}_{k=1}^{K}\right)\right]\end{aligned} \tag{6}$$

where

$$\tilde{s}(t) = \tilde{A}(t)e^{j\tilde{\phi}(t)} \qquad 0 \le t < KT \tag{7}$$

is the approximation of the continuous-time signal $s(t)$ based on (4) and (5), $\overline{\tilde{s}(t)}$ is the complex-conjugate signal, and $\mathrm{Re}\{\cdot\}$ denotes the real part. The first two terms in (6) represent the estimator-correlator for the complex signal $\tilde{s}(t)$ normalised by the noise level and $p\left(\{A_k, \phi_k, f_k, \}_{k=1}^{K}\right)$ is the prior probability density of the signal parameters. Note that our approach differs from the algorithm described in [10] in that it uses both magnitude and phase information, and the approach in [10] uses magnitude only. Moreover, our algorithm utilises a denser time-frequency grid for which $T\Delta f < 1$, that corresponds to a DTFT (see above), whereas in [10] $T\Delta f = 1$, which is used in a standard DFT-based short-time Fourier transform (STFT). There is also a difference in the way the amplitude in (6) is marginalised.

We substitute (4) and (5) in (7) and then use (7) in (6) to obtain

$$\begin{aligned}\log\left[\Lambda\left(\{A_k, \phi_k, f_k\}_{k=1}^{K}\right)\right] &\propto \frac{2}{\mathcal{N}_0}\sum_{k=1}^{K} A_k \mathrm{Re}\left[e^{-j\phi_k}\int_0^{T} x(t+kT)e^{-j2\pi f_k t}dt\right] \\ &- \frac{T}{\mathcal{N}_0}\sum_{k=1}^{K} A_k^2 + \log\left[p\left(\{A_k, \phi_k, f_k\}_{k=1}^{K}\right)\right].\end{aligned} \tag{8}$$

The amplitude A_k is assumed to be an independent random variable with a uniform prior pdf in the range $[0\ A_{max}]$, where this range covers all possible values of A_k [9]. Since this prior is constant in the range of A_k, it is irrelevant for the maximisation of $\Lambda\left(\{A_k, \phi_k, f_k, \}_{k=1}^{K}\right)$ and can be ignored in (8). To facilitate the maximisation of $\Lambda\left(\{A_k, \phi_k, f_k, \}_{k=1}^{K}\right)$, we marginalise (8) with respect to the amplitude (note that $\hat{A}_k$ can be easily computed once the values $\hat{\phi}_k$ and $\hat{f}_k$ that maximise the marginalised posterior pdf are known). The marginalisation is performed by evaluating the following integral:

$$I_k = \int_0^{A_{max}} e^{\left(\frac{2X_k}{\mathcal{N}_0}A_k - \frac{T}{\mathcal{N}_0}A_k^2\right)} dA_k \tag{9}$$

for $k = 1, \ldots, K$, where

$$X_k = \mathrm{Re}\left[e^{-j\phi_k}\int_0^{T} x(t+kT)e^{-j2\pi f_k t}dt\right] \tag{10}$$

and by letting let $A_{max} \to \infty$ [9]. The resulting equation is given by

$$I_k = \sqrt{\frac{\pi\mathcal{N}_0}{4T}}e^{\frac{X_k^2}{\mathcal{N}_0 T}}\left[1 + \mathrm{erf}\left(\frac{X_k}{\sqrt{\mathcal{N}_0 T}}\right)\right] \tag{11}$$

and the derivation of (11) is presented in the Appendix. We then use (11) to obtain the marginalised log-posterior as

$$\log\left[\Lambda\left(\{\phi_k, f_k\}_{k=1}^K\right)\right] \propto \sum_{k=1}^{K}\left(\frac{X_k^2}{\mathcal{N}_0 T} + \log\left[1+\text{erf}\left(\frac{X_k}{\sqrt{\mathcal{N}_0 T}}\right)\right]\right) + \log\left[p\left(\{\phi_k, f_k\}_{k=1}^K\right)\right] \quad (12)$$

where the constant $\sqrt{\frac{\pi\mathcal{N}_0}{4T}}$ in (11) is ignored.

C. DISCRETE-TIME POSTERIOR DISTRIBUTION FOR PHASE-FREQUENCY ESTIMATION

Thus far, we derived (12) for the continuous-time signal $x(t)$. Practical applications use the sampled version of $x(t)$ given by

$$x(l) = x(l\tau), \qquad l = 1, \ldots, KN \quad (13)$$

where τ is the sampling interval, $\tau = \frac{T}{N}$, $f_{sampl} = \frac{1}{\tau}$ is the sampling frequency, and $x(t)$ is appropriately pre-filtered using an antialiasing filter. Using the sampled signal in (13), the integral in (10) can be approximated as

$$\int_0^T x(t+kT)e^{-j2\pi f_k t} \approx \tau \sum_{l=0}^{N-1} x(l+kN)e^{-j2\pi f_k l\tau} \quad (14)$$

where the summation on the right-hand side is a complex coefficient that corresponds to the DTFT of the kth signal segment calculated at the frequency $f_k = \zeta_j \in \mathcal{F}$. The discrete-time counterpart of X_k in (10) can be defined as

$$Y_k = \text{Re}\left[e^{-j\phi_k}\sum_{l=0}^{N-1} x(l+kN)e^{-j2\pi f_k l\tau}\right] \quad (15)$$

$$= \text{Re}\left[e^{j(\psi_k-\phi_k)}B_k\right] = \cos(\psi_k-\phi_k)B_k \quad (16)$$

where B_k and ψ_k denote the magnitude and phase of the DTFT coefficient, respectively.

In (16), ϕ_k is the actual signal phase at the beginning of the kth time segment, and $\psi_k + 2l\pi$ is its estimate obtained using the DTFT at the discrete frequency $f_k = \zeta_j$, where the term $2l\pi$, $l = 0, \pm1, \pm2, \ldots$, takes into account the ambiguity of the phases with some multiple of 2π. As discussed above, the signal frequency varies continuously over the DTFT frequency-time bin $\Delta f \times N\tau$ centred at f_k, and it is generally different from f_k. Moreover, the signal may be contaminated by noise. These effects cause a decrease in the accuracy of the estimation of ϕ_k. Denote by ϑ_k the phase error due to the difference between the actual signal frequency and the closest DTFT frequency $\zeta_i \in \mathcal{F}$, and by χ_k the distortion caused by random noise. Then, the relationship between the true signal phase and its DTFT estimate is given by

$$\psi_k = \phi_k + \vartheta_k + \chi_k - 2l\pi. \quad (17)$$

We choose the parameters Δf and $T = N\tau$ that define the width and length of the DTFT bin to alleviate the effect of the phase error ϑ_k (see above). Regarding the phase error due to noise χ_k, its probability density, for white Gaussian noise, is an even function that peaks at zero; its variance and tails increase as the SNR is decreased, tending to a uniform distribution for very low SNRs [31].

We assume that the DTFT phase ψ_k can be taken as an approximation of ϕ_k, i.e.,

$$\phi_k \approx \psi_k + 2l\pi, \quad l = 0, \pm1, \pm2, \ldots. \quad (18)$$

Moreover, as discussed above, the actual signal phase ϕ_k at time step k can be predicted from phase ϕ_{k-1} at the previous time step $k-1$ as

$$\phi_k = \phi_{k-1} + 2\pi f_k N\tau. \quad (19)$$

Then, noting that the variance of the discrete-time complex white Gaussian noise is given by $\sigma_n^2 = \frac{\mathcal{N}_0 f_{sampl}}{2} = \frac{\mathcal{N}_0}{2\tau}$ and that $X_k \approx \tau Y_k$ in (16), the discrete-time version of the marginalised log-posterior (12) can be obtained as

$$\log\left[\Lambda\left(\{\phi_k, f_k\}_{k=1}^K\right)\right] \propto \sum_{k=1}^{K}\left(\frac{Y_k^2}{2N\sigma_n^2} + \log\left[1+\text{erf}\left(\frac{Y_k}{\sqrt{2N}\sigma_n}\right)\right]\right) + \log\left[p\left(\{\phi_k, f_k\}_{k=1}^K\right)\right]. \quad (20)$$

Substituting (18) and (19) in (16), we obtain Y_k in (20) as

$$Y_k \approx \cos\left(\psi_k - \psi_{k-1} - 2\pi f_k N\tau\right) B_k \quad (21)$$

where the term $2l\pi$ is omitted since cosine is a periodic function with period 2π. The use of the approximation (18)-(19) at a low SNR is facilitated by the fact that the logarithm term in the marginalised log-posterior distribution suppresses the log-likelihood ratios with a large phase estimation error, i.e., for which $\cos(\psi_k - \psi_{k-1} - 2\pi f_k N\tau) < 0$.

According to our model, the frequency f_k depends on the frequency at the previous time interval f_{k-1} and can be assumed to be independent of the frequencies f_{k-m} at the time steps $k-m$, $m > 1$. Similarly, the phase ϕ_k depends only on the phase ϕ_{k-1} and the frequency f_{k-1}. Therefore, a first-order Markov model can be appropriately used to represent the phase-frequency prior probabilities in (20) as

$$p\left(\{\phi_k, f_k\}_{k=1}^K\right) = p(\phi_1, f_1)\prod_{l=2}^{K} p(\phi_l, f_l|\phi_{l-1}, f_{l-1}) \quad (22)$$

where $p(\phi_1, f_1)$ is the prior probability at $k = 1$, and $p(\phi_l, f_l|f_{l-1}, \phi_{l-1})$ is the transition probability at $k = l$. Let $f_k = \zeta_j$ at time step k and $f_{k-1} = \zeta_i$ at time step $k-1$. Since the frequency change over a time-frequency bin is bounded as described above, the transition probabilities are restricted as follows:

$$p(\phi_k, f_k|\phi_{k-1}, f_{k-1}) = \begin{cases} p_{j|i}: & j-i \in [-1, 0, 1] \\ 0: & \text{otherwise.} \end{cases} \quad (23)$$

That is, the frequency can transition to $f_k = \zeta_j$ at the time step k only if it had one of the values (or states) ζ_i,

$i \in [j-1, j, j+1]$ at the time step $k-1$. The corresponding discrete phase state is $\phi_k = \phi_{k-1} + 2\pi\zeta_i N\tau$. Therefore, given the frequency state ζ_i at time $k-1$, the nonzero transition probabilities are restricted to $p_{j|i}$, $|j-i| \leq 1$. In general, these probabilities depend on the frequency and phase values but are independent of time since the Markov model is assumed to be homogeneous.

III. IMPLEMENTATION OF THE PROPOSED ALGORITHM

Assuming that the frequency range of interest is given by $\mathcal{F}$, the goal is to find the sequence of the parameters (or track) $\{\hat{\phi}_k, \hat{f}_k\}_{k=1}^K$ that maximises the posterior $\Lambda\left(\{\phi_k, f_k\}_{k=1}^K\right)$. The globally optimal estimate of this sequence is obtained by using the Viterbi algorithm [2], [5], [29], whereas the sequence that maximises the probability of the parameters at each time step, given the observation sequence at all time steps, is produced by the forward-backward algorithm [1], [2], [5]. These algorithms also compute a statistic that is used for signal detection. The Viterbi algorithm calculates the so-called Viterbi score as the maximum of the posterior function related to the optimal track, whereas the forward-backward algorithm evaluates the detection statistic as the sum of the likelihoods (SOL) of all possible track combinations [2].

Due to the restrictions on the transition probabilities of the Markov model (23), the Viterbi and forward-backward algorithms take simple forms. However, these algorithms use the DTFT phase and magnitude information, so their implementation differs from the standard magnitude-only versions described in [1]–[3], [5]. Here, we briefly present our application of these algorithms. Note that the objective function in (20) is given in logarithmic form, so we use a logarithmic version of the Viterbi algorithm, where the multiplications of the probabilities are replaced by the summations of the logarithms. By contrast, the forward-backward algorithm is applied to $\Lambda\left(\{\phi_k, f_k\}_{k=1}^K\right)$, which is obtained as the exponent of (20).

Define the $J \times K$ measurement structure on which the algorithms operate, where J is the number of phase-frequency states and K is the number of time steps. Each node of the structure, indexed by (j, k), is characterised by the magnitude $B_{j,k}$ and phase $\psi_{j,k}$ computed by applying the length-N DTFT on the signal segment at the time step $k \in \{1, \ldots, K\}$ and at the frequency $\zeta_j \in \mathcal{F}$, $j \in [1, \ldots, J]$. Note that for $\zeta_j \in \mathcal{F}$ and N, $\Delta f N\tau < 1$, where $\Delta f = \zeta_j - \zeta_{j-1}$ is the frequency increment. Therefore, this measurement structure is denser and contains more compact signal information compared to the one obtained using the standard STFT for which $\Delta f N\tau = 1$. Additionally, setting the parameters Δf and N so that $\Delta f N\tau < 1$ allows for a reliable use of the DTFT phase in phase-frequency tracking, as discussed above.

At the time step $k = 1$, we compute $Q_{j,1}$ as

$$Q_{j,1} = \frac{B_{j,1}^2}{2N\sigma_n^2} \tag{24}$$

TABLE 1. Viterbi algorithm for phase-frequency tracking.

for each state $j = 1, \ldots, J$ **do**
  $\mathcal{L}(j) = Q_{j,1} + \log(p_{j,1})$
  $\mathcal{R}(j, 1) = 0$
end for
for each time step $k = 2, \ldots, K$ **do**
  $\mathcal{L}' = \mathcal{L}$
  for each state $j = 1, \ldots, J$ **do**
    for each $d \in D_j$ **do**
      $V(d) = \mathcal{L}'(j+d) + Q_{j,k,d} + \log(p_{j|j+d})$
    end for
    $\mathcal{L}(j) = \max_{d \in D} [V(d)]$
    $\arg = \arg\max_{d \in D} [V(d)]$
    $\mathcal{R}(j, k) = j + \arg$
  end for
end for
return: $\mathcal{L}, \mathcal{R}$

and calculate $Y_{j,k,d}$, $k \in \{2, \ldots, K\}$, in (21), as

$$Y_{j,k,d} = \cos\left(\psi_{j,k} - \psi_{j+d,k-1} - 2\pi\zeta_{j+d}N\tau\right) B_{j,k} \tag{25}$$

where $j+d$ and j are the state indices at two consecutive time steps. Using (25), the value of $Q_{j,k,d}$ related to the kth term in the summation in (20) is given by

$$Q_{j,k,d} = \frac{\left(Y_{j,k,d}\right)^2}{2N\sigma_n^2} + \log\left[1 + \operatorname{erf}\left(\frac{Y_{j,k,d}}{\sqrt{2N}\sigma_n}\right)\right]. \tag{26}$$

The prior probabilities at $k = 1$ are defined as $p(\phi_1, \zeta_j) = p_{j,1}$, and the transition probabilities of the Markov model for the structure are set to

$$p(\phi_k, \zeta_j | \phi_{k-1}, \zeta_{j+d}) = \begin{cases} p_{j|j+d}, & d \in [-1, 0, 1] \\ 0, & \text{otherwise} \end{cases} \tag{27}$$

for $j = 1, \ldots, J$ and $k = 2, \ldots, K$, $\phi_k = \phi_{k-1} + 2\pi\zeta_{j+d}N\tau$.

The pseudocodes for the Viterbi and forward-backward algorithms are given in Tables 1 and 2, respectively. The two algorithms have the same inputs, the $J \times K$ structure with the measured DTFT magnitudes and phases, the prior probabilities at $k = 1$, $\{p_{j,1}\}_{j=1}^J$, and the transition probabilities of the Markov model given in (27). The values of $Q_{j,1}$ and $Q_{j,k,d}$ in Tables 1 and 2 are computed using (24) and (25)-(26), respectively. Additionally, to mitigate the effects due to the final dimensionality of the measurement structure, the variable D_j in Tables 1 and 2 is defined for $j = 1, \ldots, J$ as follows:

$$\begin{aligned} \text{if } j = 1 \quad & \text{set } D_j = [0, 1] \\ \text{elseif } j = J \quad & \text{set } D_j = [-1, 0] \\ \text{else} \quad & \text{set } D_j = [-1, 0, 1]. \end{aligned} \tag{28}$$

The Viterbi score L_V is obtained as the maximum of the posterior function $\mathcal{L}$ in Table 1 at $k = K$ over $1 \leq j \leq J$. The optimal (or Viterbi) track is obtained by backtracking $\mathcal{R}(j, k)$

TABLE 2. Forward-backward algorithm for phase-frequency tracking.

for each state $j = 1, \ldots, J$ **do**
  $\alpha(j,1) = p_{j,1}$
end for
for each time step $k = 2, \ldots, K$ **do**
  for each state $j = 1, \ldots, J$ **do**
    $\alpha(j,k) = \sum_{d \in D_j} \alpha(j+d, k-1) \exp(Q_{j,k,d})\, p_{j|j+d}$
  end for
end for
for each state $j = 1, \ldots, J$ **do**
  $\beta(j,K) = 1$
end for
for each time step $k = K-1, \ldots, 1$ **do**
  for each state $j = 1, \ldots, J$ **do**
    $\beta(j,k) = \sum_{d \in D_j} \beta(j+d, k+1) \exp(Q_{j+d,k+1,-d})\, p_{j|j-d}$
  end for
end for
for each time step $k = 1, \ldots, K$ **do**
  for each state $j = 1, \ldots, J$ **do**
    $\gamma(j,k) = \frac{\alpha(j,k)\beta(j,k)}{\sum_{j=1}^{J} \alpha(j,k)\beta(j,k)}$
  end for
end for
return: α, γ

starting from $R_V(K) = \mathcal{R}(j_K^*, K)$ at $k = K$, where $j_K^* = \arg\max_{1 \le j \le J} [\mathcal{L}(j)]$, and by proceeding as

$$R_V(k) = \mathcal{R}(R_V(k+1), k), \quad k = K-1, \ldots, 1. \tag{29}$$

For the forward-backward algorithm, the SOL statistic is computed as $L_{FB} = \sum_{j=1}^{J} \alpha(j,K)$, where α in Table 2 is the forward variable. The phase-frequency track is obtained as the most likely parameter state at time step k

$$R_{FB}(k) = \arg\max_{1 \le j \le J} [\gamma(j,k)], \quad k = 1, \ldots, K, \tag{30}$$

where γ in Table 2 is the probability of being in state j at time k conditioned on the observation sequence. The recursive computation of the forward and backward variables α and β can have very large values, so these variables need to be normalised as proposed in [5] (this is not shown in Table 2).

To reduce the computational complexity of the algorithms and avoid multiple computations of $Q_{j,k,d}$ in (26), the values of $Q_{j,k,d}$ are precomputed and stored in a $3 \times J \times (K-1)$ lookup table. We also compute J values for $Q_{j,1}$ in (24). The computational complexity then depends on the complexity of the DTFT measurement structure, the complexity of the $Q_{j,k,d}$ lookup table and the initial vector $Q_{j,1}$, and on the complexity of the computation carried out by the individual algorithms. The complexity of the DTFT is JKN complex multiplications and additions. The complexity of the lookup table and of the initial vector is $Jc_1 + 3J(K-1)c_2$, where c_1 and c_2 are the complexities of computing individual values of $Q_{j,1}$ and $Q_{j,k,d}$, respectively. Since the Viterbi algorithm uses summations, its complexity is $6J(K-1)$ additions, and there are also $J(K-1)$ maximisation operations. In the forward-backward algorithm, the multiplications in the computation of $\alpha(j,k)$ and $\beta(j,k)$ are implemented as a summation of logarithms, followed by applying the exponential function. These computations consist of $12J(K-1)$ additions, $6J(K-1) + 2JK$ computations of the exponential function and $2J(K-1)$ computations of the logarithmic function. Additionally, JK multiplications and divisions are required to compute γ.

IV. SIMULATION RESULTS

This section presents the results of a simulation study involving two signal types with different frequency variabilities in additive white Gaussian noise. The signals denoted by $\mathcal{TS}_1$ and $\mathcal{TS}_2$ have the frequency variability parameter $\beta_1 = 0.393$ and $\beta_2 = 0.098$, respectively, and the corresponding characteristic time intervals and frequency changes are given by $T_{s1} = 4$s and $\Delta f_{s1} = 0.25$ Hz and $T_{s2} = 8$s and $\Delta f_{s2} = 0.125$ Hz. The signal frequency is assumed to obey a stochastic process driven by white noise. Consequently, it evolves continuously and has nondeterministic fluctuations. For both signals, we set $\Delta f = 0.1$ Hz and define the time extension T of the frequency time bin (or the length of the DTFT) as $T \approx \frac{\Delta f}{\Delta f_{s1}} T_{s1}$, where $T = N\tau$, $\tau = \frac{1}{f_{sampl}}$ and f_{sampl} is the sampling frequency. This choice of Δf and T is suitable for both the signal with the higher frequency variability $\mathcal{TS}_1$ and the signal with the lower variability $\mathcal{TS}_2$.

The frequency of the signal $\mathcal{TS}_i$, $i = 1, 2$, is modelled as being continuous with a piecewise linear change over consecutive time intervals T, and the slope is uniformly distributed in the range $\left[-\frac{\Delta f_i}{T}\ \ \frac{\Delta f_i}{T}\right]$, $\Delta f_i = \Delta f_{si} \frac{T}{T_{si}}$. This model is used to generate synthetic complex signals based on (1)-(2) in the Monte Carlo simulations, with the signal amplitude A being constant over the duration of the signal and the initial frequency being uniformly distributed in the range [400 Hz 420 Hz].

The SNR for the bandwidth determined by the sampling frequency is defined using the equivalent real-valued signal with the amplitude $2A$ as $SNR = 10 \log_{10}\left(2A^2/\sigma_n^2\right)$. For the noise in the frequency bandwidth of interest (20 Hz), the SNR is defined as $SNR_{20Hz} \approx SNR + 20$ dB.

We denote the two versions of the algorithm described in this paper as PF-FB and PF-Vit, where the extension 'FB' represents the use of the forward-backward algorithm and the extension 'Vit' indicates the use of the Viterbi algorithm. For comparison, we used the methods described by Barrett and Holdsworth [4] that utilise the magnitude and phase information denoted by PF-BH-FB and PF-BH-Vit, the magnitude-only methods proposed by Paris and Jaufret [5] denoted by F-PJ-FB and F-PJ-Vit, and a method based on (20) where we disregard the phase and use only the magnitude, denoted by F-Vit. An algorithm that uses both the phase and magnitude has also been considered in [9], but insufficient information about this approach is given in [9], and it could not be replicated here.

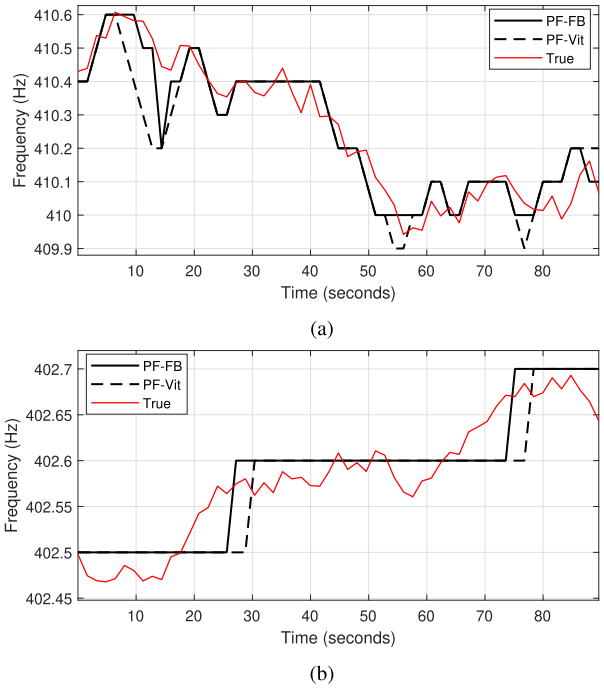

FIGURE 1. The true signal frequency and the estimated (reconstructed) frequency at $SNR = -32$ dB obtained using the phase-frequency methods PF-FB and PF-Vit described in this paper for a synthetic test signal of types (a) $\mathcal{TS}_1$ and (b) $\mathcal{TS}_2$.

All the algorithms are applied to the DTFT data structure described in Section III. The approaches described in [4] require knowledge of the amplitude, and we set this amplitude to $A = 1$. Additionally, the data likelihood proposed in [4] is used in a similar manner as described in this paper.

Since the frequency of the simulated signals is modelled as a stochastic process, the transition probabilities of the Markov chain used in the tested algorithms are computed based on the joint phase-frequency pdf described in [9], where the parameters σ and γ in [9] are set to $\sigma = \Delta f_i$, $i = 1, 2$, and $\gamma = 10^{-5}$. The exceptions are the methods described in [5] that use the transition probabilities defined in [5].

We evaluate the detection and frequency tracking performance of all algorithms based on 5000 Monte Carlo runs at a given SNR, where each run used a separate random realisation of the signal. The detection results are presented by plotting the probability of detection P_D against the probability of false alarm P_{FA} at a range of threshold levels. The detection statistic is the Viterbi score L_V for the methods using the Viterbi algorithm and the SOL statistic L_{FB} for the methods based on the forward-backward algorithms. The threshold levels for false alarm probabilities are determined by running the algorithms on a large number of noise-only data series and by recording the detection statistics. We also measure the deviation between the true (actual) signal frequency and the frequency track estimated by the algorithm using the mean-square error (MSE) defined as

$$MSE = \frac{1}{KN}\sum_{l=1}^{KN}\left(f_{true}(l) - \tilde{f}(l)\right)^2. \tag{31}$$

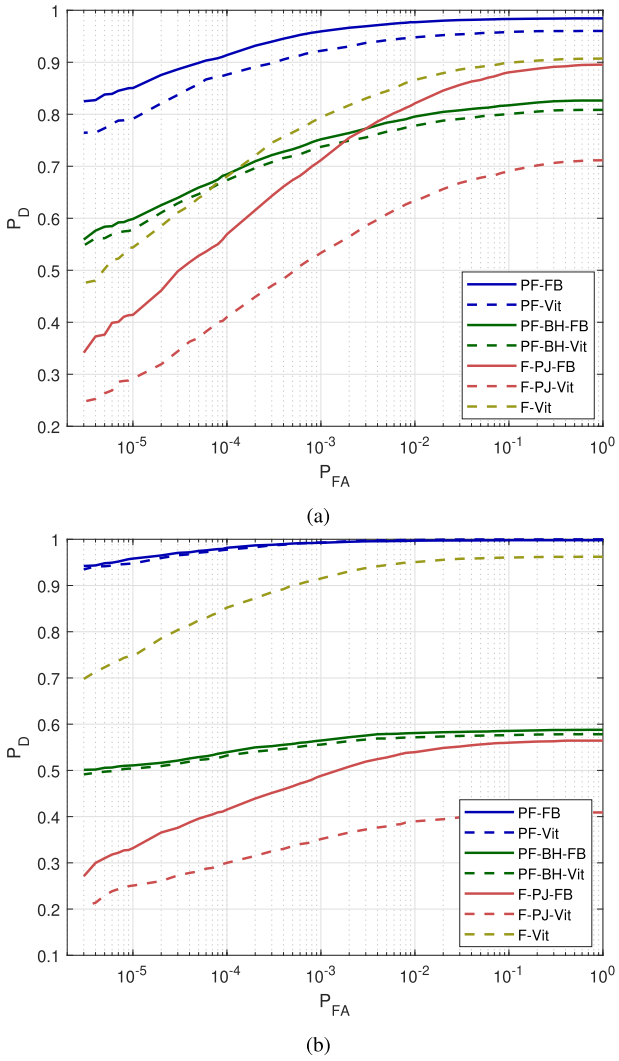

FIGURE 2. Probability of detection P_D as a function of the probability of false alarm P_{FA} for all tested methods at $SNR = -32$ dB for the synthetic signal types (a) $\mathcal{TS}_1$ and (b) $\mathcal{TS}_2$.

In (31), $f_{true}(l)$ is the true frequency of the sampled synthetic signal, and $\tilde{f}(l)$ is the frequency reconstructed based on the discrete tracks R_V (29) and R_{FB} (30) using a piecewise-linear model. The detection is considered successful if the detection statistic computed by the algorithm is higher than a given threshold *and* if the MSE between the true signal frequency and the reconstructed frequency is smaller than the threshold $\mathcal{W}_i = [\Delta f_{si}]^2$, where for the test signal $\mathcal{TS}_i$, $i = 1, 2$, $\Delta f_{s1} = 0.25$ Hz and $\Delta f_{s2} = 0.125$ Hz, respectively.

Figs. 1 (a) and (b) show examples of the true signal frequency and the estimated frequency at $SNR = -32$ dB obtained using the phase-frequency methods PF-FB and PF-Vit for the synthetic signals with different frequency variabilities $\mathcal{TS}_1$ and $\mathcal{TS}_2$, respectively.

The probability of detection P_D as a function of the probability of false alarm P_{FA} for the tested algorithms and for the two signal types at $SNR = -32$ dB is shown in Figs. 2 (a) and (b). From Fig. 2 (b), it can be seen that

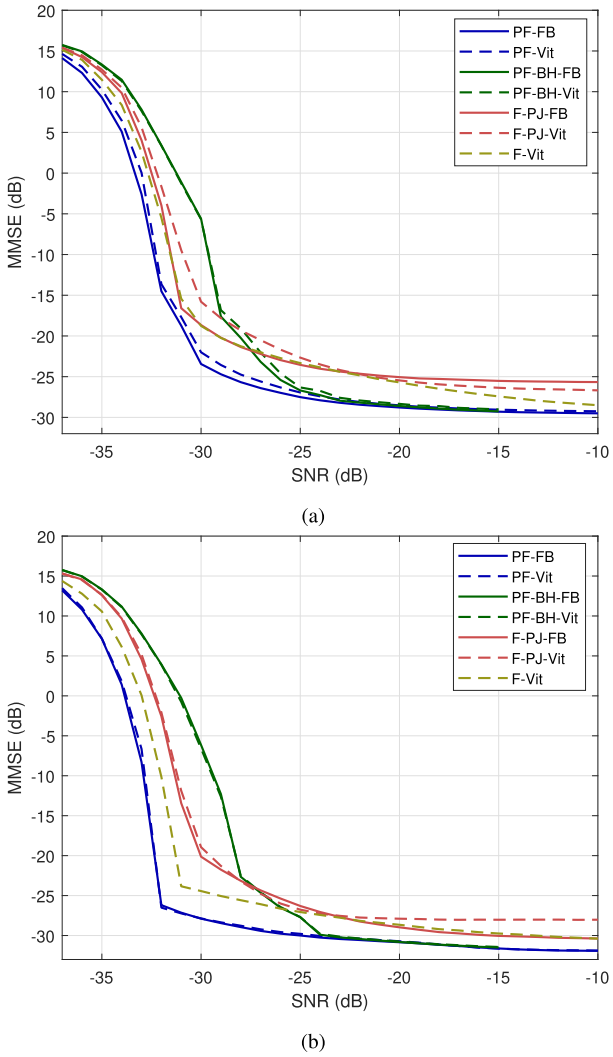

FIGURE 3. MMSE for the random frequency tracking for all tested methods for the synthetic signal types (a) $\mathcal{TS}_1$ and (b) $\mathcal{TS}_2$.

the detection performance of the methods [4] and [5] deteriorates for the signals with the lower frequency variability $\mathcal{TS}_2$ compared to the performance of the higher frequency variability signals $\mathcal{TS}_1$. The reason is that the MSE threshold $\mathcal{W}_2 = [0.125]^2$ is smaller than the threshold $\mathcal{W}_1 = [0.25]^2$, so a larger number of detections of the signal $\mathcal{TS}_2$ are disregarded since their corresponding MSE was higher than the threshold compared to the results obtained using the test signal $\mathcal{TS}_1$. Additionally, the amplitude used by the algorithms [4] differed from the actual signal amplitude, which further affected the performance of these methods. By contrast, the algorithms PF-FB and PF-Vit described in this paper display both good detection rates and high frequency tracking accuracy. We note that the probabilities of detection P_D in Figs. 2 (a) and (b) can be smaller than $P_D = 1$ for $P_{FA} = 1$. This is because there are a number of estimated track MSEs at $P_{FA} = 1$ that are greater than the MSE threshold $\mathcal{W}_i$, which lowers the detection probability as explained above.

TABLE 3. Relative computational times of the tested algorithms.

Method	PF	PF-BH	PF-PJ	F
Viterbi	1.00	1.08	1.39	0.97
Forward-Backward	0.96	1.04	1.94	-

To further evaluate the frequency tracking performance of the algorithms, we compute the mean MSE (MMSE) over the MSEs of $M = 5000$ Monte Carlo runs as

$$MMSE = 10\log_{10}\left(\frac{1}{M}\sum_{m=1}^{M} MSE_m\right). \tag{32}$$

Figs. 3 (a) and (b) show the plot of the MMSE against a range of SNRs for the signal types $\mathcal{TS}_1$ and $\mathcal{TS}_2$, respectively.

To compare the computational complexity of the tested algorithms, we use the average computational time of each algorithm relative to the average computational time of the Viterbi algorithm PF-Vit described in this paper. The algorithms are implemented in MATLAB [32] and run on a personal computer under the Windows 10 operating system, and the results are shown in Table 3. The approaches that are used for comparison with the proposed algorithms are implemented in a similar way as our algorithms (see Section III). Therefore, the computational complexity of these approaches includes the complexity of the DTFT measurement structure, the complexity of the lookup table, and the complexity of computing the variables of the individual algorithms. It is interesting to note that, contrary to the expectation, the computational complexity of the phase-frequency Viterbi algorithms PF-Vit and PF-BH-Vit is higher than the computational complexity of the respective forward-backward algorithms, PF-FB and PF-BH-FB. These differences are related to the computational complexity of the algorithms themselves. In particular, the Viterbi algorithms utilise a maximisation operation that is more computationally costly than the exponential and logarithmic functions used by the forward-backward algorithms, and the complexity of the maximisation operation contributes to the increased computational time of the phase-frequency Viterbi algorithms. The algorithms PF-PJ-Vit and PF-PJ-FB described in [5] require much longer computational times than the other tested algorithms, while the computational complexity of the magnitude-only Viterbi algorithm F-Vit is lower than that of PF-Vit because F-Vit relies only on the DTFT magnitudes and does not utilise the phases.

From the results shown in Figs. 2 and 3 and in Table 3, it can be seen that the proposed phase-frequency algorithms perform consistently better than several existing frequency detection and tracking methods in terms of the frequency estimation accuracy and detection rate at low SNRs and the computational complexity. We note that in this study, the frequency variability of the signal was known, so we were able to accurately compute the transition probabilities of the Markov model. In realistic situations, the exact signal frequency variability is not always known, although it may

be known that it belongs to a range of values, and this can affect the performance of the algorithms. However, this may influence only the accuracy of the transition probabilities of the Markov chain but not the accuracy of the signal segment likelihoods. For this reason, it is not expected that in this case, the performance of the algorithms would significantly decline. An approach to alleviate this problem would be to simultaneously track the signal frequency and estimate its frequency variability, improving the accuracy of the estimation of the transition probabilities.

V. CONCLUSION

This paper presented an approach to the problems of detection and tracking of a random-frequency signal in additive complex white Gaussian noise. Two detection/tracking algorithms were proposed that used the DTFT magnitude and phase information and allowed for refined phase-frequency detection and tracking. The transition of the discrete phase-frequency states was modelled using a first-order homogeneous Markov sequence, and the transition probabilities of the Markov chain were computed using an approach described in [9]. A comprehensive simulation study involving two signal types with different frequency variabilities was carried out. The results show that the proposed trackers/detectors perform significantly better than several existing frequency detection and tracking methods.

APPENDIX. EVALUATION OF THE INTEGRAL FOR THE MARGINALISATION OF THE POSTERIOR DISTRIBUTION

Here, we present the evaluation of the following integral

$$\begin{aligned} I_k &= \int_0^{A_{max}} e^{(\frac{2X_k}{\mathcal{N}_0}A_k - \frac{T}{\mathcal{N}_0}A_k^2)} dA_k \\ &= \int_0^{A_{max}} e^{-(\frac{T}{\mathcal{N}_0}A_k^2 - \frac{2X_k}{\mathcal{N}_0}A_k)} dA_k. \end{aligned} \tag{33}$$

We use the completion of the square of the quadratic $ax^2 + bx + c$ given by

$$f(x) = ax^2 + bx + c = a(x-h)^2 + g \tag{34}$$

where $h = -\frac{b}{2a}$ and $g = f(h) = ah^2 + bh + c$. Additionally, $e^{a(x-h)^2+g} = e^g e^{a(x-h)^2}$, where e^g is a constant. Therefore, the integral we need to evaluate becomes

$$\begin{aligned} I &= \int_0^{X_{max}} e^{-[a(x-h)^2+g]} dx \\ &= e^{-g} \int_0^{X_{max}} e^{-a(x-h)^2} dx \end{aligned} \tag{35}$$

where $a = \frac{T}{\mathcal{N}_0}$, $b = -\frac{2X_k}{\mathcal{N}_0}$, $c = 0$, $h = \frac{X_k}{T}$, $g = -\frac{X_k^2}{\mathcal{N}_0 T}$, $x = A_k$ and $X_{max} = A_{max}$.

We first evaluate the integral

$$I' = \int_0^{X_{max}} e^{-a(x-h)^2} dx \tag{36}$$

where we define the substitution $y = x - h$. Then, $x = y + h$ and $dx = dy$. The upper limit of the integral is $X_{max} - h$, and the lower limit of the integral is $-h$. Then, I' becomes

$$I' = \int_{-h}^{X_{max}-h} e^{-ay^2} dy. \tag{37}$$

We use the following properties of the erf function:

$$\int_p^q e^{-ay^2} dy = \frac{1}{2}\frac{\sqrt{\pi}}{\sqrt{a}}\Big[\text{erf}(q\sqrt{a}) - \text{erf}(p\sqrt{a})\Big], \tag{38}$$

$$\text{erf}(-z) = -\text{erf}(z), \tag{39}$$

and

$$\text{erf}(\infty) = 1 \tag{40}$$

where

$$\text{erf}(z) = \frac{2}{\sqrt{\pi}} \int_0^z e^{-y^2} dy. \tag{41}$$

Using (38) and (39) in (37), we obtain

$$\begin{aligned} I' &= \frac{\sqrt{\pi}}{2\sqrt{a}}\Big[\text{erf}((X_{max}-h)\sqrt{a}) - \text{erf}(-h\sqrt{a})\Big] \\ &= \frac{\sqrt{\pi}}{2\sqrt{a}}\Big[\text{erf}((X_{max}-h)\sqrt{a}) + \text{erf}(h\sqrt{a})\Big]. \end{aligned} \tag{42}$$

Setting $X_{max} \to \infty$ and using (40), (42) becomes

$$I' = \frac{\sqrt{\pi}}{2\sqrt{a}}\Big[1 + \text{erf}(h\sqrt{a})\Big]. \tag{43}$$

Substituting (43) and the corresponding parameter values in (33), we obtain for I_k

$$I_k = \sqrt{\frac{\pi\mathcal{N}_0}{4T}} e^{\frac{X_k^2}{\mathcal{N}_0 T}} \left[1 + \text{erf}\left(\frac{X_k}{\sqrt{\mathcal{N}_0 T}}\right)\right]. \tag{44}$$

REFERENCES

[1] L. Rabiner and B. Juang, "An introduction to hidden Markov models," *IEEE ASSP Mag.*, vol. ASSP-3, no. 1, pp. 4–16, Jan. 1986.

[2] L. R. Rabiner, "A tutorial on hidden Markov models and selected applications in speech recognition," *Proc. IEEE*, vol. 77, no. 2, pp. 257–286, Feb. 1989.

[3] R. L. Streit and R. F. Barrett, "Frequency line tracking using hidden Markov models," *IEEE Trans. Acoust., Speech Signal Process.*, vol. 38, no. 4, pp. 586–598, Apr. 1990.

[4] R. F. Barrett and D. A. Holdsworth, "Frequency tracking using hidden Markov models with amplitude and phase information," *IEEE Trans. Signal Process.*, vol. 41, no. 10, pp. 2965–2976, Oct. 1993.

[5] S. Paris and C. Jauffret, "Frequency line tracking using HMM-based schemes," *IEEE Trans. Aerosp. Electron. Syst.*, vol. 39, no. 2, pp. 439–449, Apr. 2003.

[6] G. Pulford and K. Tyson, "A high performance 1-D hidden Markov model tracker for passive sonar systems," in *Proc. Undersea Defence Technol.*, Rotterdam, The Netherlands, Apr. 2015, pp. 1–20.

[7] S. Suvorova, L. Sun, A. Melatos, W. Moran, and R. Evans, "Hidden Markov model tracking of continuous gravitational waves from a neutron star with wandering spin," *Phys. Rev. D, Part. Fields*, vol. 93, no. 12, 2016, Art. no. 123009.

[8] S. Suvorova, P. Clearwater, A. Melatos, L. Sun, W. Moran, and R. Evans, "Hidden Markov model tracking of continuous gravitational waves from a binary neutron star with wandering spin. II. Binary orbital phase tracking," *Phys. Rev. D, Part. Fields*, vol. 96, no. 10, 2017, Art. no. 102006.

[9] S. Suvorova, A. Melatos, R. J. Evans, W. Moran, P. Clearwater, and L. Sun, "Phase-continuous frequency line track-before-detect of a tone with slow frequency variation," *IEEE Trans. Signal Process.*, vol. 66, no. 24, pp. 6434–6442, Dec. 2018.

[10] R. Short and J. P. Toomey, "Detection and estimation of frequency-random signals," *IEEE Trans. Inf. Theory*, vol. IT-6, no. 28, pp. 940–946, Nov. 1982.
[11] T. Luginbuhl and P. Willett, "Estimating the parameters of general frequency modulated signals," *IEEE Trans. Signal Process.*, vol. 52, no. 1, pp. 117–131, Jan. 2004.
[12] D. Carevic and S. Davey, "Two algorithms for modeling and tracking of dynamic time-frequency spectra," *IEEE Trans. Signal Process.*, vol. 64, no. 22, pp. 6030–6045, Nov. 2016.
[13] G. L. Ogden, L. M. Zurk, M. E. Jones, and M. E. Peterson, "Extraction of small boat harmonic signatatures from passive sonar," *J. Acoust. Soc. Amer.*, vol. 129, no. 6, pp. 3768–3776, 2011.
[14] W. Ng, C. ji, W.-K. Ma, and H. C. So, "A study on particle filters for single-tone frequency tracking," *IEEE Trans. Aerosp. Electron. Syst.*, vol. 45, no. 3, pp. 1111–1123, Jul. 2009.
[15] W. Ng, "Multiple-model based particle filters for frequency tracking in α stable noise," *IEEE Trans. Aerosp. Electron. Syst.*, vol. 47, no. 3, pp. 2254–2261, Jul. 2011.
[16] S. Peleg and B. Friedlander, "The discrete polynomial-phase transform," *IEEE Trans. Signal Process.*, vol. 43, no. 8, pp. 1901–1914, Aug. 1995.
[17] S. Peleg and B. Friedlander, "Multicomponent signal analysis using the polynomial-phase transform," *IEEE Trans. Aerosp. Electron. Syst.*, vol. 32, no. 1, pp. 378–387, Jan. 1996.
[18] H. M. Ozaktas, O. Arikan, M. A. Kutay, and G. Bozdagt, "Digital computation of the fractional Fourier transform," *IEEE Trans. Signal Process.*, vol. 44, no. 9, pp. 2141–2150, Sep. 1996.
[19] S.-C. Pei and J.-J. Ding, "Closed-form discrete fractional and affine Fourier transforms," *IEEE Trans. Signal Process.*, vol. 48, no. 5, pp. 1338–1353, May 2000.
[20] S. Liu, T. Shan, R. Tao, Y. D. Zhang, G. Zhang, F. Zhang, and Y. Wang, "Sparse discrete fractional Fourier transform and its applications," *IEEE Trans. Signal Process.*, vol. 62, no. 24, pp. 6582–6594, Oct. 2014.
[21] H. Zhang, T. Shan, S. Liu, and R. Tao, "Optimized sparse fractional Fourier transform: Principle and performance analysis," *Signal Process.*, vol. 174, pp. 1–12, Sep. 2020.
[22] R. Tao, Y.-L. Li, and Y. Wang, "Short-time fractional Fourier transform and its appliactions," *IEEE Trans. Signal Process.*, vol. 58, no. 5, pp. 2568–2580, May 2010.
[23] C. Ioana, J. Mars, A. Serbanescu, and S. Stankovic, "Time-frequency-phase tracking approach: Application to underwater signals in passive context," in *Proc. IEEE Int. Conf. Acoust., Speech Signal Process. (ICASSP)*, Dallas, TX, USA, Mar. 2010, pp. 3401–3404.
[24] F. Dadouchi, J. W. Pitton, C. Ioana, and C. Gervaise, "Time-frequency tracking using multi-window local phase analysis," in *Proc. IEEE Int. Conf. Acoust., Speech Signal Process. (ICASSP)*, Kyoto, Japan, Mar. 2012, pp. 3397–3400.
[25] C. Ioana, C. Gervaise, Y. Stéphan, and J. I. Mars, "Analysis of underwater mammal vocalisations using time–frequency-phase tracker," *Appl. Acoust.*, vol. 71, no. 11, pp. 1070–1080, Nov. 2010.
[26] S. Liu, T. Shan, Y. D. Zhang, R. Tao, and Y. Feng, "A fast algorithm for multi-component LFM signal analysis exploiting segmented DPT and SDFrFT," in *Proc. IEEE Radar Conf. (RadarCon)*, Arlington, VA, USA, May 2015, pp. 1139–1143.
[27] M. F. McKenna, D. Ross, S. M. Wiggins, and J. A. Hildebrand, "Underwater radiated noise from modern commercial ships," *Acoust. Soc. Amer.*, vol. 131, no. 1, pp. 92–103, Jan. 2012.
[28] S. Liu, Y. D. Zhang, and R. Tao, "Structure-aware Bayesian compressive sensing for frequency-hopping spectrum estimation with missing observations," *IEEE Trans. Signal Process.*, vol. 66, no. 8, pp. 2153–2165, Apr. 2018.
[29] G. D. Forney, "The Viterbi algorithm," *Proc. IEEE*, vol. 61, no. 3, pp. 219–227, Mar. 1977.
[30] H. V. Trees, *Detection, Estimation and Modulation Theory*, vol. 1. New York, NY, USA: Wiley, 1968.
[31] D. Middleton, *An Introduction to Statistical Communication Theory*. New York, NY, USA: McGraw-Hill, 1960.
[32] *MATLAB Version 9.10.0.1613233 (R2021a)*, Mathworks, Natick, MA, USA, 2021.

DRAGANA CAREVIC received the B.Eng. and M.Sc. degrees in electrical engineering from Belgrade University, Belgrade, Yugoslavia, and the Ph.D. degree in computer science from Curtin University, Bentley, WA, Australia, in 1996.

In 1996, she joined the Defence Science and Technology Group, Edinburgh, SA, Australia, where she carried out research into land mine detection. Since 1999, she has been with the Maritime Division, Defence Science and Technology Group, Rockingham, WA, Australia. Her current research interests include Bayesian statistics, multiple model estimation, sensor fusion, and tracking.